OPEN

Intrinsic noise alters the frequency spectrum of mesoscopic oscillatory chemical reaction systems

Rajesh Ramaswamy & Ivo F. Sbalzarini

MOSAIC Group, Institute of Theoretical Computer Science, ETH Zurich, CH–8092 Zürich, Switzerland.
Swiss Institute of Bioinformatics, ETH Zurich, CH–8092 Zürich, Switzerland.

Mesoscopic oscillatory reaction systems, for example in cell biology, can exhibit stochastic oscillations in the form of cyclic random walks even if the corresponding macroscopic system does not oscillate. We study how the intrinsic noise from molecular discreteness influences the frequency spectrum of mesoscopic oscillators using as a model system a cascade of coupled Brusselators away from the Hopf bifurcation. The results show that the spectrum of an oscillator depends on the level of noise. In particular, the peak frequency of the oscillator is reduced by increasing noise, and the bandwidth increased. Along a cascade of coupled oscillators, the peak frequency is further reduced with every stage and also the bandwidth is reduced. These effects can help understand the role of noise in chemical oscillators and provide fingerprints for more reliable parameter identification and volume measurement from experimental spectra.

I n mesoscopic reaction systems the copy numbers of the reacting molecules are low enough for molecular discreteness to become relevant. This induces intrinsic noise and replaces the deterministic kinetics by a stochastic model, potentially leading to quantitative and qualitative differences in the system behavior.

Oscillatory chemical reaction networks are appealing systems to study as they can exhibit a wide range of complex behaviors, such as bifurcations, limit cycles, and chaos in different parts of their phase spaces. Consequently, they have been shown to be involved in a number of fundamental phenomena, including pattern formation[1], turbulence[2,3], chemical waves[3], and vortex dynamics[4]. Chemical oscillators also play important roles in biological systems, ranging from circadian clocks[5,6] to rhythmic gene expression and metabolism[7], glycolytic oscillators[8], embryonic segmentation clocks[9], and cell-division control in both space and time[10–12].

Oscillatory chemical reaction networks have traditionally been studied using deterministic, macroscopic reaction rate equations (RRE) in the form of ordinary differential equations. While this enables the application of a wealth of bifurcation and stability analysis tools from dynamical systems theory, it is only valid in the limit of large numbers of molecules, which typically requires that the reactions progress in a reactor of large (macroscopic) volume[13–15]. If the reactions are confined to smaller (mesoscopic) volumes, such as intracellular organelles, nano-reactors, or porous foams, the number of reactive molecules within any well-mixed subspace is typically too small for RRE to be generally valid. In these regimes, molecular discreteness, and hence intrinsic noise, needs to be accounted for. It has been shown in numerous studies that intrinsic noise can lead to non-trivial chemical kinetics that cannot be predicted by RRE[15–21].

The effect of intrinsic noise manifests itself differently in different types of chemical reaction networks: In linear reaction networks RRE predictions of the mean concentrations are always correct, regardless of the reactor volume[14]. In nonlinear reaction networks, however, noise induces quantitative differences from the concentrations predicted by RRE[14,15]. A fingerprint of these differences is the relaxation kinetics of the steady-state concentration fluctuations[22]. In monostable nonlinear systems, the relaxation kinetics of the concentration fluctuations around a non-equilibrium steady state is altered by intrinsic noise through an increase in the lifetimes of species that are reactants in any nonlinear reaction[22]. In frequency space, this corresponds to an increase in the bandwidth of the concentration fluctuation spectrum with increasing intrinsic noise. This quantitative difference can become large enough to render RRE invalid in certain regimes[20]. In multi-stable systems, intrinsic noise can lead to switching behavior between the multiple fixed points of the system[14,15]. This phenomenon has been used to explain spontaneous switching behavior in biochemical systems[23–25] and the switching of gene-expression patterns in response to environmental changes[26]. More remarkably, intrinsic noise can induce oscillatory behavior at

steady state, even when the corresponding RRE are away from Hopf bifurcation and hence do not exhibit oscillatory behavior[27,21]. This has, e.g., been used to explain circadian rhythms in biological organisms[28,5,6].

Analysis and prediction of noise-induced effects in multi-stable and oscillatory systems is impeded by the fact that many analytical methods, such as van Kampen's system-volume expansion[15] or the effective mesoscopic rate equations (EMRE)[29], are limited to asymptotically (in a Lyapunov sense) monostable systems[15]. Consequently, understanding mesoscopic oscillatory systems requires other theoretical approaches, such as the stochastic normal form equations[30], Gaussian approximation methods[31], the Mori-Zwanzig projection method[32], or the Hamilton-Jacobi method[33,34]. These methods have been used to understand stochastic fluctuations around a limit cycle in the weak-noise limit, and they have led to a wealth of results about the radius of the limit cycle, correlation times, and the minimum number of molecules required for sustained time-correlated oscillations.

All these approaches are based on approximations of the chemical master equation (CME)[35], which governs the stochastic kinetics of chemical reaction networks in mesoscopic and macroscopic volumes. While analytically intractable, the CME renders these systems amenable to simulation studies by numerically sampling trajectories from the exact solution of the CME using an exact stochastic simulation algorithm (SSA)[36]. These algorithms are exact in the sense that they reproduce the correct fluctuation spectrum of the species concentrations to arbitrarily high order.

In this paper, we use an exact SSA and a mesoscopic oscillatory model system away from Hopf bifurcation to characterize the effect of intrinsic noise on the frequency spectrum of the steady-state concentration fluctuations. Extending previous work on monostable systems[22], we study the fingerprints of noise in the frequency spectrum of the stochastic chemical oscillations as a function of the magnitude of intrinsic noise. For this, we study the fluctuation–relaxation kinetics of the concentrations of species in an open, mesoscopic chemical model system. We use Gillespie's original exact SSA[36] to sample trajectories governed by the corresponding CME. The impact of noise is quantified by changes in the power spectral density (PSD) of the concentration fluctuations at a non-equilibrium steady state. Larger intrinsic noise is realized by decreasing the reactor volume Ω at constant mean concentration, hence decreasing the total number of reactive molecules in the system. We observe that the PSD has a Lorentzian-like form, confirming an earlier study[30]. Further, we show that the frequency at which the PSD is maximum depends on the reactor volume and hence the noise magnitude. We observe that the peak shifts toward lower frequencies with increasing intrinsic noise. This shift is also accompanied by an increase in bandwidth of the fluctuation spectrum, similar to the observation in monostable systems[22].

Interactions between several oscillatory systems may lead to non-trivial effects[37]. We hence also study cascades of downstream-coupled mesoscopic chemical systems and compare the results to a single-stage system and to the linear-noise regime[38,15]. We show that due to intrinsic noise, each cascade stage further amplifies the shift in the peak of the PSD toward lower frequencies. For a fixed volume, the bandwidth decreases along the cascade, rendering the peak sharper and more relevant with every additional stage. In biology, downstream-coupled cascades of reaction networks are found, e.g., as cascades of autocatalytic reactions or in signaling cascades. This includes the up to six downstream-coupled autocatalytic stages of MAPK signaling cascades[39,40], which can exhibit oscillatory behavior under global feedback[41]. Another example of an oscillatory autocatalytic biochemical system is found in cell cycle control[11,12].

We believe that our findings shed light on the effect of intrinsic noise on mesoscopic oscillatory chemical reaction systems. We show that intrinsic noise can not only induce oscillatory behavior in systems away from Hopf bifurcation[27,21], but that it also alters the frequency spectrum of the oscillations. The key novelty in our findings is the shift of the peak of the Lorentzian-like PSD with increasing intrinsic noise. Our findings can be used to understand the fundamental effects of intrinsic noise in (cascades of) mesoscopic chemical reaction networks. Furthermore, it has been shown that steady-state fluctuation spectra can aid parameter identification of stochastic chemical reaction networks[42]. Under this premise, our results can be used to more reliably identify the parameters of mesoscopic chemical reaction networks by using the corrected fluctuation–relaxation kinetics as an additional fingerprint of the effects of intrinsic noise, where the time series of steady-state fluctuations can, e.g., be obtained using fluorescence correlation spectroscopy (FCS)[43–45].

Results

Model. We consider a chain of dowstream-coupled Brusselators[38] in a reactor of volume Ω (see Fig. 1) as a model system. The Brusselator is a model system for autocatalytic reactions. Examples of autocatalytic reactions include the Belousov-Zhabotinsky reaction, MAPK signaling cascades[39,40], and activation of the M-phase promoting factor in cell-cycle control[11,12]. The reaction network of our model system is:
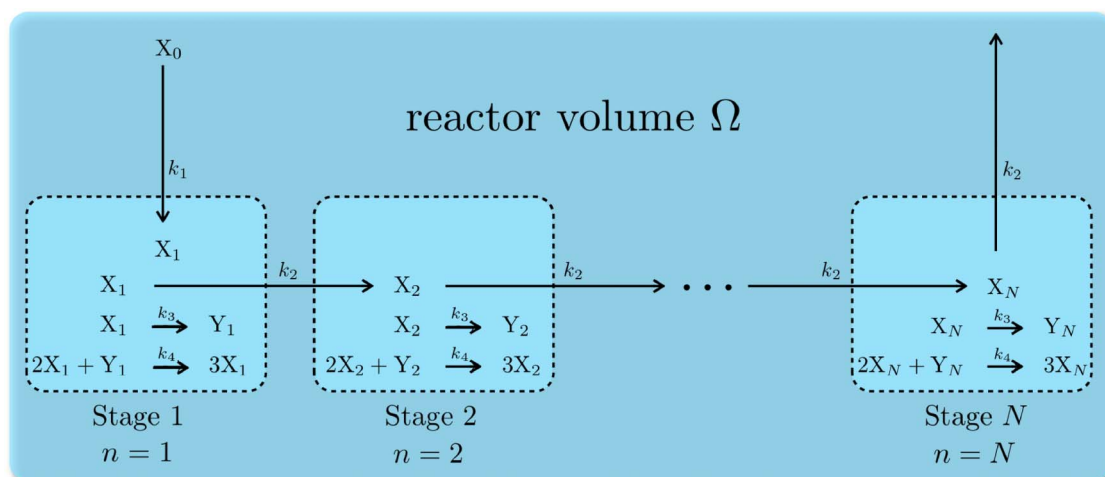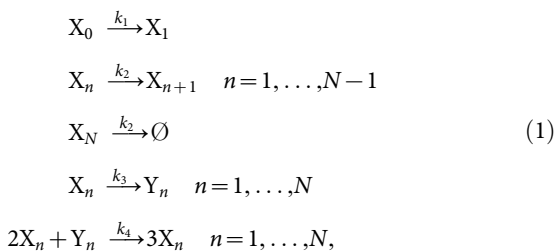

Figure 1 | Illustration of the model system of a cascade of *N* downstream-coupled Brusselators. The cascade of Brusselator reactions progresses in a mesoscopic reactor volume Ω.

$$X_0 \xrightarrow{k_1} X_1$$

$$X_n \xrightarrow{k_2} X_{n+1} \quad n = 1, \ldots, N-1$$

$$X_N \xrightarrow{k_2} \varnothing \tag{1}$$

$$X_n \xrightarrow{k_3} Y_n \quad n = 1, \ldots, N$$

$$2X_n + Y_n \xrightarrow{k_4} 3X_n \quad n = 1, \ldots, N,$$

where n denotes the stage of the cascade and $N \geq 1$ the total number of stages. The k's are the macroscopic reaction rates. Each stage $n \geq 1$ involves reactions between two species, X_n and Y_n. The first stage of the cascade is driven by a buffer (species X_0) whose concentration is fixed at all times. Every subsequent stage of the cascade is driven by species X_{n-1} of the previous stage. Therefore, the first stage $n = 1$ is independent of the subsequent downstream stages ($n > 1$). In general, any stage $n = q$ is independent of all the subsequent downstream stages ($n > q$).

The CME corresponding to the reaction system in Eq. 1 is given by

$$\frac{\partial P(X_1, Y_1)}{\partial t} = x_0 \Omega k_1 \left(E_{X_1}^{-1} - 1 \right) P(X_1, Y_1) + k_2 \left(E_{X_1}^{1} - 1 \right) X_1 P(X_1, Y_1)$$
$$+ k_3 \left(E_{X_1}^{1} E_{Y_1}^{-1} - 1 \right) X_1 P(X_1, Y_1) + \frac{k_4}{\Omega^2} \left(E_{X_1}^{-1} E_{Y_1}^{1} - 1 \right) X_1 (X_1 - 1) Y_1 P(X_1, Y_1)$$

$$\frac{\partial P(X_n, Y_n)}{\partial t} = k_2 \left(E_{X_n}^{1} - 1 \right) X_n P(X_n, Y_n) + k_3 \left(E_{X_n}^{1} E_{Y_n}^{-1} - 1 \right) X_n P(X_n, Y_n)$$
$$+ \frac{k_4}{\Omega^2} \left(E_{X_n}^{-1} E_{Y_n}^{1} - 1 \right) X_n (X_n - 1) Y_n P(X_n, Y_n), \quad n = 2, \ldots, N, \tag{2}$$

where X_n and Y_n are the populations (copy numbers) of species X_n and Y_n, respectively, x_0 is the concentration of the buffer X_0, $P(X_n, Y_n)$ is the probability of having X_n molecules of species X_n and Y_n molecules of species Y_n, and E_X is a step operator defined as $E_X^m f(X, Y) = f(X + m, Y)$ for any function $f(\cdot)$. The corresponding RRE describing the deterministic time evolution of the concentrations $x_n = X_n/\Omega$ and $y_n = Y_n/\Omega$ is given in Eq. 6 (see Methods section).

For simplicity, we set $k_2 = k_4 = 1$. We also enforce the concentration x_0 of the buffer X_0 to be 1 at all times. Under these conditions, the fixed point of the deterministic RRE (Eq. 6) is given by $x_n(t \to \infty) = k_1$ and $y_n(t \to \infty) = k_3/k_1$ for all $n \geq 1$. This fixed point is exponentially stable if $k_3 < k_1^2 + 1$, undergoes a Hopf bifurcation at $k_3 = k_1^2 + 1$, and becomes unstable for $k_3 > k_1^2 + 1$. In the latter case, $x_n(t)$ and $y_n(t)$ exhibit oscillations for each $n = 1, \ldots, N$. In the deterministic RRE description, the condition for a limit cycle has to be strictly fulfilled in order to observe oscillatory behavior, whereas in the stochastic description oscillations can be observed even when the limit-cycle condition is not fulfilled[27,5].

We numerically sample trajectories from the CME (Eq. 2) using the direct method[46], an exact formulation of Gillespie's stochastic simulation algorithm[36], for different reactor volumes Ω. The reactor volume determines the magnitude of intrinsic noise, as smaller Ω decrease the total number of reactive molecules in the system and hence increase the intrinsic noise magnitude. We set $N = 20$, thus simulating a cascade of 20 Brusselator stages, which includes the single-stage case when looking at the concentrations in stage 1, since they are independent of any subsequent stages. This value for N is chosen arbitrarily and the results would not change if a different N were chosen. The concentrations of all species are 0 at time $t = 0$. We also set $k_1 = 1$ and $k_3 = 1$. For these parameters, the fixed point of the system is stable, and the deterministic system does hence not exhibit limit-cycle oscillations, reaching the fixed point $(x_n, y_n) = (1,1)$ for all $n = 1, \ldots, N$. The mesoscopic system, however, shows oscillations due to the concentration fluctuations from intrinsic noise. This can be seen in Fig. 2, where the deterministic RRE trajectories from the first and last cascade stages are shown in panels (b) and (d), respectively, and a single trajectory sampled from the CME in panels (a) and (c). Starting from the above initial condition, the stochastic trajectory

shows sustained oscillations, whereas the deterministic trajectory reaches the stable fixed point.

We study the normalized steady-state PSD $S_n(\omega)$ of the concentration fluctuations of species X_n (species X of the n-th stage) for $n = 1, \ldots, N$ as a function of the angular frequency ω for different reactor volumes Ω. The normalized steady-state PSD $S_n(\omega)$ is defined as the Fourier transform of the time-autocorrelation function $C_n(\tau)$:

$$S_n(\omega) = \mathcal{F}(C_n(\tau)), \tag{3}$$

where the time autocorrelation in function of the time lag τ is given by

$$C_n(\tau) = \langle \tilde{x}_n(0) \tilde{x}_n(\tau) \rangle_s / \sigma_n^2. \tag{4}$$

The subscript s denotes quantities computed at steady state, $\tilde{x}_n = x_n - \langle x_n \rangle_s$, and the variance at steady state $\sigma_n^2 = \langle \tilde{x}_n(0) \tilde{x}_n(0) \rangle_s$. The normalization of $C_n(\tau)$ with σ_n^2 factors out the energy of the fluctuations, so that $\int_0^\infty S_n(\omega) d\omega = 1$. We hence call $S_n(\omega)$ the *normalized steady-state PSD*. It quantifies the fraction of energy of the fluctuations around a specific frequency, namely, $S_n(\omega) d\omega$ gives the fraction of energy of the fluctuations between ω and $\omega + d\omega$. We compute $S_n(\omega)$ by recording a single long trajectory of $x_n(t)$ at steady state. We sample 8 404 992 ($2^{23} + 2^{14}$) data points of $x_n(t)$ starting from $t = 2000$ with a time resolution of $\delta t = 0.1$. We then compute the time-autocorrelation function (Eq. 4) from a minimum lag of $\tau = 0.1$ up to a maximum lag of $\tau = 2^{14} \delta t$. $S_n(\omega)$ is obtained by fast Fourier transform (Eq. 3).

We quantify the effect of intrinsic noise by the PSD's peak frequency and bandwidth. The peak frequency ω_n^m is defined as the angular frequency at which $S_n(\omega)$ is maximum, hence

$$\omega_n^m = \arg \max_\omega (S_n(\omega)). \tag{5}$$

Since $S_n(\omega)$ is generated by a stochastic process and hence is noisy, we smooth $S_n(\omega)$ before computing ω_n^m. Smoothing is done using a moving-average filter with a window diameter of 10 data points, corresponding to a frequency-space resolution of $\delta\omega = 2 \cdot 10^{-2}$ (data points in frequency space are uniformly spaced with a distance of $2 \cdot 10^{-3}$).

The bandwidth ω_n^b of the steady-state PSD is defined as the difference between the two frequencies (ω_1, ω_2) where the steady-state PSD drops to half of its maximum value, i.e., $\omega_n^b = \omega_2 - \omega_1$ so that $S_n(\omega_1) = S_n(\omega_2) = \frac{1}{2} S_n(\omega_n^m)$ with $\omega_2 > \omega_1$. Also ω_n^b is computed on the smoothed PSD.

In the linear-noise (large volume) regime, the quantities $S_n(\omega)$ and ω_n^m can be calculated analytically[38,15] (see Methods section). We use the results from the linear-noise regime as a baseline to understand the effect of intrinsic noise on our model system.

Effect of noise. We present the normalized steady-state PSD $S_n(\omega)$, the peak frequency ω_n^m, and the bandwidth ω_n^b for different reactor volumes Ω of our model system. These quantities are numerically computed from exact SSA trajectories[46,35] as described above. In the linear-noise limit, the quantities are analytically computed as described in the Methods section.

First, we assess $S_n(\omega)$ as a function of reactor volume Ω for the stage $n = 1$ alone and then extend our results to cascades of coupled Brusselators. Figure 3(a) shows $S_1(\omega)$ for three different reactor volumes $\Omega = 1, 5, 50$ and in the linear-noise limit. It can be seen that the steady-state PSD is indeed a function of Ω and that it has a Lorentzian-like form with a peak frequency and an associated bandwidth. This form of the steady-state PSD is expected, since the time-autocorrelation function is $C_n(t) \propto e^{-\alpha_n t} \cos(\beta_n t)$ [30]. As the volume Ω is reduced, the peak ω_1^m shifts to lower frequencies. The linear-noise regime is the weak-noise limit for large Ω. For $\Omega = 50$ the peak frequency is $\omega_1^n = 0.86$. This reduces to $\omega_1^m = 0.73$ and $\omega_1^m = 0.45$ for $\Omega = 5$ and $\Omega = 1$, respectively.
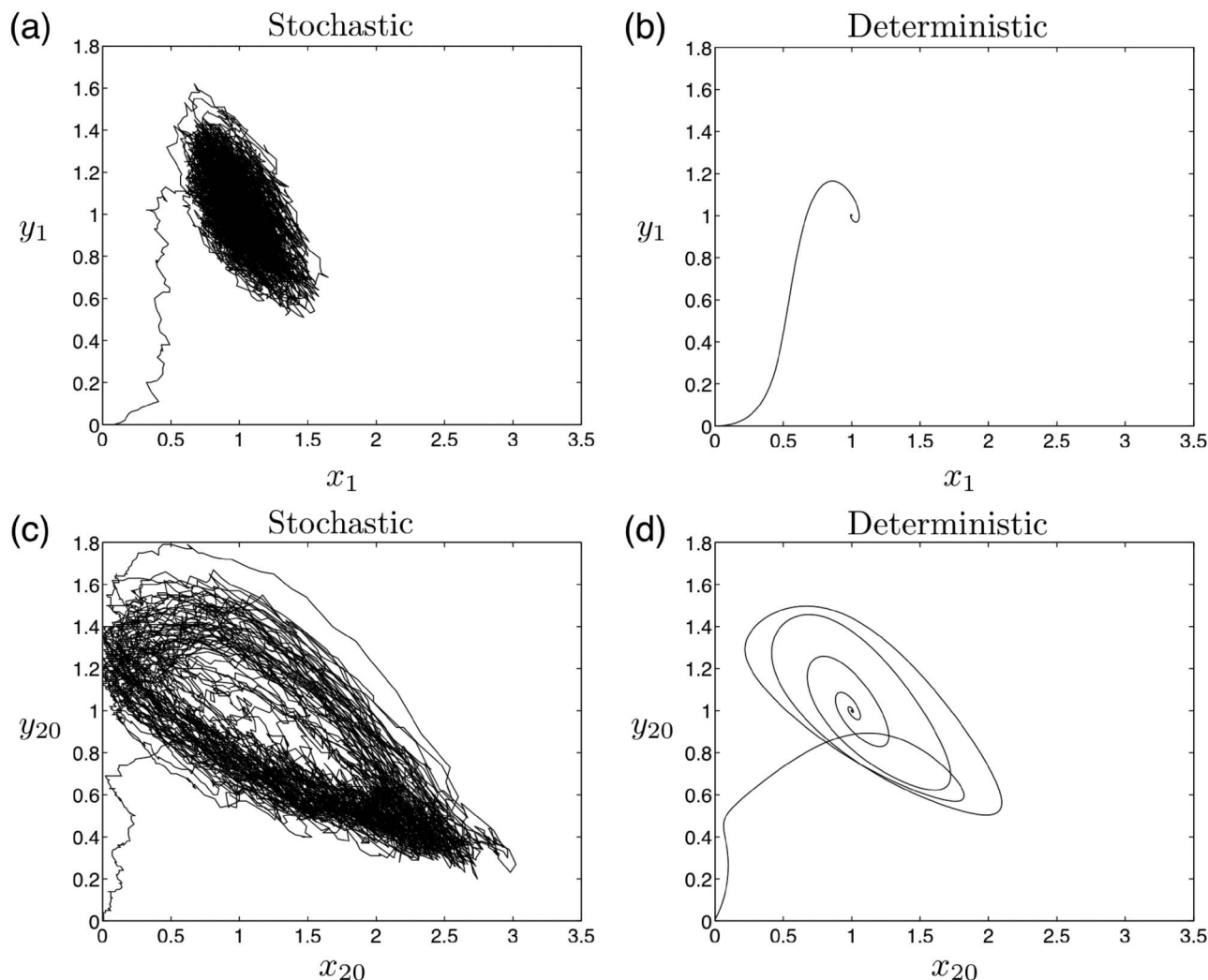
Figure 2 | Plot of a single trajectory in phase space (x_n, y_n) for the first and last stages, $n = 1$ and $n = 20$, of the model system (Eq. 1) with $N = 20$ and reactor volume $\Omega = 100$. For this system, the RRE predict an exponentially stable fixed point at $(x_n, y_n) = (1, 1)$. (a) A single stochastic trajectory sampled from the CME for stage $n = 1$; (b) the corresponding deterministic RRE prediction for the same parameters. (c, d) Stochastic and deterministic trajectories, respectively, for the last stage of the cascade.

The bandwidth for $\Omega = 50$ is $\omega_1^{\mathrm{b}} = 1.19$. For $\Omega = 5$, it increases to $\omega_1^{\mathrm{b}} = 1.29$, and for $\Omega = 1$ further to $\omega_1^{\mathrm{b}} = 1.46$. The bandwidth of the steady-state PSD hence increases with decreasing reactor volume Ω.

We now consider how these results change along a cascade of downstream-coupled Brusselators. Figure 3(b) shows $S_{20}(\omega)$ at stage $n = 20$ for the same three reactor volumes $\Omega = 1, 5, 50$ and in the linear-noise limit. Similar to what is observed in the first stage, the peak ω_{20}^{m} also shifts toward lower frequencies as Ω decreases. For $\Omega = 50$ the peak frequency is $\omega_{20}^{\mathrm{m}} = 0.72$, which reduces to $\omega_{20}^{\mathrm{m}} = 0.51$ and $\omega_{20}^{\mathrm{m}} = 0.28$ for $\Omega = 5$ and $\Omega = 1$, respectively. For a given Ω, the peak frequency is successively reduced by each cascade stage, hence $\omega_{n+1}^{\mathrm{m}} < \omega_n^{\mathrm{m}}$.

The bandwidth ω_n^{b} at stage $n = 20$ also increases with decreasing volume, just as it did for the first stage (see Fig. 3(b)). For $\Omega = 50, 5$, and 1, we find $\omega_{20}^{\mathrm{b}} = 0.37$, $\omega_{20}^{\mathrm{b}} = 0.48$, and $\omega_{20}^{\mathrm{b}} = 0.50$, respectively. Comparing ω_1^{b} and ω_{20}^{b}, we observe that for fixed reactor volume Ω the bandwidth *decreases* with every stage along the cascade.

These results are summarized in Table 1 and shown also for intermediate cascade stages in Fig. 4. We observe that for a given cascade stage n the peak frequency decreases with decreasing reactor volume and that for a given reactor volume the peak frequency also decreases with every stage along the cascade. In the linearized approximation (valid for large volumes), the peak frequency is independent of the reactor volume and also of the cascade stage (see Eq. 14). This

indicates that the effects observed for smaller volumes are indeed caused by intrinsic noise in the system.

Discussion

We have studied the effect of intrinsic noise due to molecular discreteness on mesoscopic oscillatory chemical reaction networks. We considered the model system of a Brusselator away from the Hopf bifurcation, where the deterministic reaction rate equations (RRE) do not exhibit oscillatory behavior. Oscillations can nevertheless be induced by intrinsic noise, the magnitude of which was tuned by changing the reactor volume. We also studied propagation of noise-induced effects along a downstream-coupled cascade of Brusselators. Noise-induced effects were quantified using the frequency spectrum of concentration fluctuations, given by the normalized power spectral density (PSD), at a non-equilibrium steady state. Specifically, we used the peak frequency and the bandwidth of the PSD as fingerprints of noise-induced effects. We used an exact stochastic simulation algorithm[46,35] to study the kinetics of the system as governed by the corresponding chemical master equation.

The results have shown that the frequency at which the steady-state PSD is maximal decreases with decreasing reactor volume. This effect is further amplified by every stage of a cascade of coupled Brusselators, leading to a further decrease along the cascade. This
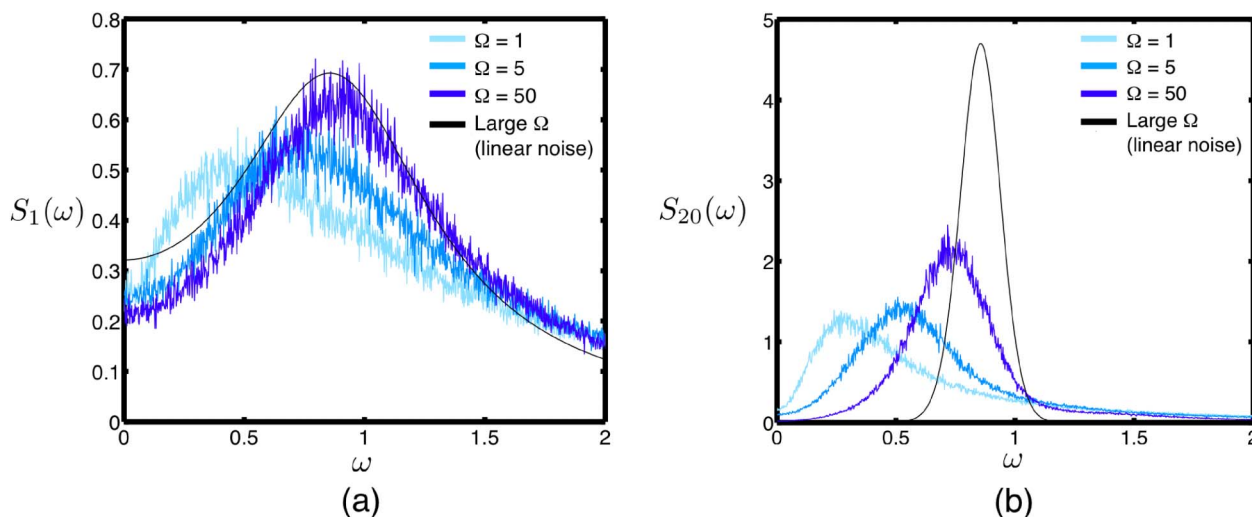
Figure 3 | Effect of intrinsic noise on the frequency spectrum of non-equilibrium steady-state concentration fluctuations. (a) Normalized steady-state power spectral density $S_1(\omega)$ of the fluctuations of species X_1 (see Eq. 3) for a single Brusselator in different reactor volumes $\Omega = 1, 5, 50$ and in the linear-noise limit for large, macroscopic Ω (see Methods section), the latter reflecting the baseline. (b) Normalized steady-state power spectral density $S_{20}(\omega)$ of the fluctuations of species X_{20} at the last stage of a cascade of 20 downstream-coupled Brusselators in different reactor volumes $\Omega = 1, 5, 50$ and in the linear-noise limit for large Ω.

is in contrast to the linearized approximation, which does not predict any effect of intrinsic noise on the *normalized* steady-state PSD. We also showed that for a given cascade stage the bandwidth of concentration fluctuations decreases with increasing reactor volume, which is in agreement with observations in non-oscillatory monostable[22] and oscillatory[34,30] chemical reaction systems. For a fixed volume, the bandwidth also decreases along the cascade, rendering the peak sharper and more pronounced with every stage. One may hence speculate whether intrinsic noise plays any role in "tuning" the output frequency of biochemical oscillators. This tuned output frequency could in turn drive further downstream reaction networks, qualitatively changing their behavior. It is for example known that the behavior of glycolytic oscillators can change from periodic to quasi-periodic to chaotic upon small changes in the driving input frequency (see p. 33, Fig. 2.24, in Ref. 47, or Refs. 48, 49).

We believe that our study sheds light on the role of intrinsic noise in chemical oscillators. Even though we studied a simple model system, the results show how intrinsic noise qualitatively influences the frequency spectrum of the oscillations. We have shown that mesoscopic chemical reaction networks, and cascades thereof, exhibit different output spectra depending on the magnitude of intrinsic noise. We expect this effect to be present also in mesoscopic oscillatory reaction systems where the RRE show oscillatory behavior. This is because there is no qualitative difference in the concentration trajectories of mesoscopic systems just before and after a Hopf bifurcation[27].

Our findings are relevant for identifying the reactor volumes of (cascades of) mesoscopic reaction networks when the concentration fluctuations are measured experimentally, e.g., using fluorescence correction spectroscopy. In addition, we believe that the effects reported here can be used as fingerprints to more reliably identify parameters of stochastic chemical reaction networks in systems biology models. Finally, the results presented here might contribute towards developing a general understanding of how noise influences the kinetics of different chemical systems, when deterministic RRE predictions are valid, and what deviations are to be expected otherwise.

Methods

Flutuations around the linearized RRE. We analytically derive the normalized steady-state PSD $S_n(\omega)$ and its peak frequency ω_n^m for each cascade stage n in the linear-noise regime. The derivation follows that of Shibata [38] and is valid in the weak-noise limit at large (macroscopic) volumes Ω.
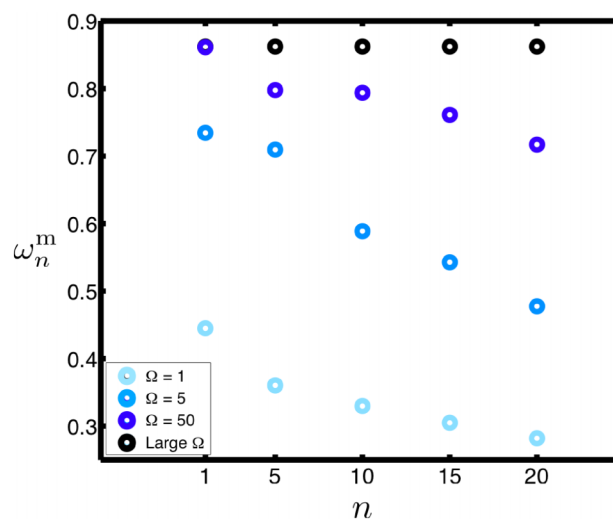

Figure 4 | Peak frequency ω_n^m of the normalized steady-state power spectral density $S_n(\omega)$ as a function of cascade stage n in different reactor volumes Ω. The results for "large Ω" are obtained from the analytical expressions in the linear-noise limit (see Methods section).

Table 1 | The effect of intrinsic noise, realized by decreasing the reactor volume Ω, on the peak frequency ω_n^m (see Eq. 5) and the bandwidth ω_n^b of the normalized steady-state PSD $S_n(\omega)$ (see Eq. 3) for stages $n = 1$ and $n = 20$ of a cascade of downstream-coupled Brusselators (see Eq. 1).

Ω	Stage 1 ($n = 1$)		Stage 20 ($n = 20$)	
	ω_1^m	ω_1^b	ω_{20}^m	ω_{20}^b
Large (linear noise)	0.86	1.18	0.86	0.19
50	0.86	1.19	0.72	0.37
5	0.73	1.29	0.51	0.48
1	0.45	1.46	0.28	0.50

The deterministic RRE for the reaction system given in Eq. 1 are

$$\frac{dx_1}{dt} = k_1 x_0 - k_3 x_1 - k_2 x_1 + k_4 x_1^2 y_1$$

$$\frac{dx_n}{dt} = k_2 x_{n-1} - k_3 x_n - k_2 x_n + k_4 x_n^2 y_n \quad n = 2, \ldots, N \tag{6}$$

$$\frac{dy_n}{dt} = k_3 x_n - k_4 x_n^2 y_n \quad n = 2, \ldots, N,$$

where x_n and y_n are the concentrations of species X_n and Y_n, respectively. As in the numerical study for mesoscopic volumes, we set $k_2 = k_4 = x_0 = 1$. Let δx_n and δy_n be small perturbations around the steady state $(x_n, y_n) = (k_1, k_3/k_1)$. The linear equations for the perturbations around the steady state are given by

$$\begin{pmatrix} \frac{d\delta x_n}{dt} \\ \frac{d\delta y_n}{dt} \end{pmatrix} = \begin{pmatrix} k_3 - 1 & k_1^2 \\ -k_3 & -k_1^2 \end{pmatrix} \begin{pmatrix} \delta x_n \\ \delta y_n \end{pmatrix} + \begin{pmatrix} 1 & 0 \\ 0 & 0 \end{pmatrix} \begin{pmatrix} \delta x_{n-1} \\ \delta y_{n-1} \end{pmatrix}. \tag{7}$$

This expression for the perturbations around the fixed point of the RRE is the same as the one that can be obtained from the linear-noise approximation using van-Kampen expansion.

Taking the Fourier transform on both sides, we obtain

$$\begin{pmatrix} j\omega & 0 \\ 0 & j\omega \end{pmatrix} \begin{pmatrix} \mathcal{X}_n \\ \mathcal{Y}_n \end{pmatrix} = \begin{pmatrix} k_3 - 1 & k_1^2 \\ -k_3 & -k_1^2 \end{pmatrix} \begin{pmatrix} \mathcal{X}_n \\ \mathcal{Y}_n \end{pmatrix} + \begin{pmatrix} 1 & 0 \\ 0 & 0 \end{pmatrix} \begin{pmatrix} \mathcal{X}_{n-1} \\ \mathcal{Y}_{n-1} \end{pmatrix}, \tag{8}$$

where $\mathcal{X}_n$ and $\mathcal{Y}_n$ are the Fourier transforms of $x_n(t)$ and $y_n(t)$, respectively. Simplifying the above equation leads to

$$\mathcal{X}_n = F(\omega) \mathcal{X}_{n-1}, \tag{9}$$

where

$$F(\omega) = \frac{j\omega + k_1^2}{-\omega^2 + j(k_1^2 - k_3 + 1)\omega + k_1^2}. \tag{10}$$

Since we consider a linearized version of the macroscopic system, the normalized PSD is invariant to the input noise excitation used to quantify the correlations introduced by the system. We here use the simple input noise $\delta x_0 = \epsilon_0(t)$, which is uncorrelated white noise with $\langle \epsilon_0(t) \rangle = 0$ and $\langle \epsilon_0(t)\epsilon_0(t+\tau) \rangle = \sigma_0^2 \delta(\tau)$, where $\delta(\tau)$ is the Dirac delta distribution. The PSD $P_0(\omega)$ of the input buffer to the first stage is then given by

$$P_0(\omega) = \langle |\mathcal{X}_0(\omega)|^2 \rangle$$
$$= \frac{\sigma_0^2}{2\pi}. \tag{11}$$

The PSD $P_n(\omega)$ of the output of cascade stage $n \geq 1$ is given by

$$P_n(\omega) = \langle |\mathcal{X}_n(\omega)|^2 \rangle. \tag{12}$$

Substituting Eqs. 9 and 11 into Eq. 12 we get

$$P_n(\omega) = |F(\omega)|^{2n} \frac{\sigma_0^2}{2\pi}.$$

The normalized steady-state PSD $S_n(\omega)$ is then

$$S_n(\omega) = \frac{P_n(\omega)}{\int_0^\infty P_n(\omega')d\omega'}$$
$$= \frac{|F(\omega)|^{2n}}{\int_0^\infty |F(\omega')|^{2n}d\omega'}. \tag{13}$$

Given the expression for $F(\omega)$ (Eq. 10), the normalized steady-state PSD $S_n(\omega)$ has a Lorentzian-like form with peak frequency

$$\omega_n^m = \sqrt{-k_1^4 + k_1^2 \sqrt{2k_1^2 k_3 + 2k_3 - k_3^2}} \quad \forall n. \tag{14}$$

It is therefore evident that in the linear-noise regime the peak frequency ω_n^m is independent of Ω and of the stage number n. The bandwidth ω_n^b in the linear-noise limit is computed directly from Eq. 13.

1. Kuramoto, Y. and Yamada, T. Pattern formation in oscillatory chemical reactions. *Progr. Theoret. Phys.* **56**, 724–740 (1976).
2. Mertens, F., Imbihl, R., and Mikhailov, A. Turbulence and standing waves in oscillatory chemical reactions with global coupling. *J. Chem. Phys.* **101**, 9903 (1994).
3. Kuramoto, Y. *Chemical oscillations, waves, and turbulence.* Dover Publications, (2003).
4. Wu, X., Chee, M., and Kapral, R. Vortex dynamics in oscillatory chemical systems. *Chaos* **1**, 421 (1991).
5. Li, Q. and Lang, X. Internal noise-sustained circadian rhythms in a drosophila model. *Biophys. J.* **94**, 1983–1994 (2008).
6. Ko, C. H. *et al.* Emergence of noise-induced oscillations in the central circadian pacemaker. *PLoS Biol.* **8**, e1000513, October (2010).
7. Schibler, U. and Naef, F. Cellular oscillators: rhythmic gene expression and metabolism. *Curr. Opin. Cell Biol.* **17**, 223–229 (2005).
8. Hess, B. The glycolytic oscillator. *J. Exp. Biol.* **81**, 7–14 (1979).
9. Pourquié, O. The segmentation clock: converting embryonic time into spatial pattern. *Science* **301**, 328 (2003).
10. Hu, Z. and Lutkenhaus, J. Topological regulation of cell division in Escherichia coli involves rapid pole to pole oscillation of the division inhibitor MinC under the control of MinD and MinE. *Mol. Microbiol.* **34**, 82–90 (1999).
11. Novak, B. and Tyson, J. Numerical analysis of a comprehensive model of M-phase control in Xenopus oocyte extracts and intact embryos. *J. Cell Sci.* **106**, 1153–1168 (1993).
12. Tyson, J., Novak, B., Odell, G., Chen, K., and Dennis Thron, C. Chemical kinetic theory: understanding cell-cycle regulation. *Trends Biochem. Sci.* **21**, 89–96 (1996).
13. Kurtz, T. G. Relationship between stochastic and deterministic models for chemical reactions. *J. Chem. Phys.* **57**, 2976–2978 (1972).
14. Gillespie, D. T. *Markov Processes: An Introduction for Physical Scientists.* Academic Press, (1991).
15. van Kampen, N. G. *Stochastic Processes in Physics and Chemistry.* North Holland, 2nd edition, (2001).
16. Gardiner, C. W., McNeil, K. J., Walls, D. F., and Matheson, I. S. Correlations in stochastic theories of chemical-reactions. *J. Stat. Phys.* **14**, 307–331 (1976).
17. Samoilov, M. S. and Arkin, A. P. Deviant effects in molecular reaction pathways. *Nature Biotechnology* **24**, 1235–1240, October (2006).
18. Thattai, M. and van Oudenaarden, A. Intrinsic noise in gene regulatory networks. *Proc. Natl. Acad. Sci. USA* **98**, 8614–8619 (2001).
19. McAdams, H. H. and Arkin, A. It's a noisy business! genetic regulation at the nanomolar scale. *Trends Genet.* **15**, 65–69, February (1999).
20. Grima, R. Noise-induced breakdown of the Michaelis-Menten equation in steady-state conditions. *Phys. Rev. Lett.* **102**, 218103 (2009).
21. Baxendale, P. H. and Greenwood, P. E. Sustained oscillations for density dependent Markov processes. *J. Math. Biol.* **63**, 433–457 (2011).
22. Ramaswamy, R., Sbalzarini, I. F., and González-Segredo, N. Noise-induced modulation of the relaxation kinetics around a non-equilibrium steady state of non-linear chemical reaction networks. *PLoS ONE* **6**, e16045 (2011).
23. Carrier, T. and Keasling, J. Investigating autocatalytic gene expression systems through mechanistic modeling. *J. Theor. Biol.* **201**, 25–36, November (1999).
24. Tian, T. and Burrage, K. Stochastic models for regulatory networks of the genetic toggle switch. *Proc. Natl. Acad. Sci. USA* **103**, 8372–8377 (2006).
25. Samoilov, M., Plyasunov, S., and Arkin, A. P. Stochastic amplification and signaling in enzymatic futile cycles through noise-induced bistability with oscillations. *Proc. Natl. Acad. Sci. USA* **102**, 2310–2315 (2005).
26. Kashiwagi, A., Urabe, I., Kaneko, K., and Yomo, T. Adaptive response of a gene network to environmental changes by fitness-induced attractor selection. *PLoS ONE* **1**, e49 (2006).
27. Qian, H., Saffarian, S., and Elson, E. L. Concentration fluctuations in a mesoscopic oscillating chemical reaction system. *Proc. Natl. Acad. Sci. USA* **99**, 10376–10381 (2002).
28. Barkai, N. and Leibler, S. Biological rhythms - circadian clocks limited by noise. *Nature* **403**, 267–268 (2000).
29. Grima, R. An effective rate equation approach to reaction kinetics in small volumes: Theory and application to biochemical reactions in nonequilibrium steady-state conditions. *J. Chem. Phys.* **133**, 035101 (2010).
30. Xiao, T., Ma, J., Hou, Z., and Xin, H. Effects of internal noise in mesoscopic chemical systems near Hopf bifurcation. *New J. Phys.* **9**, 403 (2007).
31. Tomita, K., Ohta, T., and Tomita, H. Irreversible circulation and orbital revolution —hard mode instability in far-from-equilibrium situation—. *Prog. Theor. Phys.* **52**, 1744–1765 (1974).
32. Grossmann, S. and Schranner, R. Dynamical correlations near instabilities in nonlinear chemical reaction systems. *Z. Phys. B* **30**, 325–337 (1978).
33. Vance, W. and Ross, J. Fluctuations near limit cycles in chemical reaction systems. *J. Chem. Phys.* **105**, 479–487 (1996).
34. Gaspard, P. The correlation time of mesoscopic chemical clocks. *J. Chem. Phys.* **117**, 8905–8916 (2002).
35. Gillespie, D. T. A rigorous derivation of the chemical master equation. *Physica A* **188**, 404–425 (1992).
36. Gillespie, D. T. Exact stochastic simulation of coupled chemical reactions. *J. Phys. Chem.* **81**, 2340–2361 (1977).
37. Cohen, D. and Neu, J. Interacting oscillatory chemical reactors. *Annals of the New York Academy of Sciences* **316**, 332–337 (1979).
38. Shibata, T. Amplification of noise in a cascade chemical reaction. *Phys. Rev. E* **69**, 056218 (2004).
39. Seger, R. and Krebs, E. The MAPK signaling cascade. *The FASEB journal* **9**, 726 (1995).

40. Angeli, D., Ferrell Jr., J. E., and Sontag, E. D. Detection of multistability, bifurcations, and hysteresis in a large class of biological positive-feedback systems. *Proc. Natl. Acad. Sci. USA* **101**, 1822–1827 (2004).

41. Kholodenko, B. N. Negative feedback and ultrasensitivity can bring about oscillations in the mitogen-activated protein kinase cascades. *Eur. J. Biochem.* **267**, 1583–1588 (2000).

42. Munsky, B., Trinh, B., and Khammash, M. Listening to the noise: random fluctuations reveal gene network parameters. *Mol. Sys. Biol.* **5**, 318 (2009).

43. Lakowicz, J. R. *Principles of Fluorescence Spectroscopy.* Springer US, (2006).

44. Qian, H. and Elson, E. L. Fluorescence correlation spectroscopy with high-order and dual-color correlation to probe nonequilibrium steady states. *Proc. Natl. Acad. Sci. USA* **101**, 2828–2833 (2004).

45. Rigler, R. and Elson, E. S. *Fluorescence Correlation Spectroscopy, Theory and Applications*, volume 65 of *Springer Series in Chemical Physics.* Springer-Verlag, Heidelberg, Germany, (2001).

46. Gillespie, D. T. A general method for numerically simulating the stochastic time evolution of coupled chemical reactions. *J. Comput. Phys.* **22**, 403–434 (1976).

47. Holden, A. V. *Chaos.* Princeton University Press, (1986).

48. Tomita, K. and Daido, H. Possibility of chaotic behaviour and multi-basins in forced glycolytic oscillations. *Phys. Lett. A* **79**, 133–137 (1980).

49. Chandra, F. A., Buzi, G., and Doyle, J. C. Glycolytic oscillations and limits on robust efficiency. *Science* **333**, 187–192 (2011).

Acknowledgments

Author contributions

RR and IFS conceived the study and RR implemented and ran the simulations. RR and IFS wrote the manuscript text and RR prepared the figures. Both authors reviewed and edited the manuscript.

Additional information

How to cite this article: Ramaswamy, R. & Sbalzarini, I.F. Intrinsic noise alters the frequency spectrum of mesoscopic oscillatory chemical reaction systems. *Sci. Rep.* **1**, 154; DOI:10.1038/srep00154 (2011).